Review and Comparative Analysis of GaAs/AlGaAs And GaN/AlGaN HEMTs

Aryan Bhaskar
Department of Electrical Engineering
Indian Institute of Technology Bombay
Mumbai, India
Email: 21d070017@iitb.ac.in

Apurba Laha
Department of Electrical Engineering
Indian Institute of Technology Bombay
Mumbai, India
Email: laha@iitb.ac.in

Kushagra Gehlot
Department of Electrical Engineering
Indian Institute of Technology Bombay
Mumbai, India
Email: 21d070041@iitb.ac.in

Abstract – High Electron Mobility Transistors (HEMTs) have seen growing interest in their structure and properties owing to their superior performance in high-power and high-frequency applications compared to Si-based CMOS infrastructure. In the HEMT landscape, heterostructures based on AlGaAs/GaAs have been popular, but with recent advancements in nitride technology, AlGaN/GaN-based technology has come to the fore. In this work, we attempt a comparative analysis of the two HEMT structures, reviewing their properties and applications and taking inputs from simulations wherever possible. Simulations are carried out on National Taiwan University's DDCC solver platform.

***Index Terms*— DDCC, GaAs, GaN, HEMTs, heterostructure, MODFET, polarization, power, Poisson-Schrödinger , two-dimensional electron gas (2DEG),**

I. Introduction

Gallium nitride (GaN) and gallium arsenide (GaAs) high electron mobility transistors (HEMTs) have emerged as vital technologies in high-frequency and high-power electronics, captivating researchers in various scientific and engineering fields. Compared to traditional transistors, HEMTs show unique electronic properties, evident from their band diagrams, as seen in Figure 1. These heterostructures, with typical dimensions ranging from nanometre to micrometer length scales, bridge the gap between traditional semiconductor devices and next-generation, high-performance applications. The unique properties of GaN/AlGaN and GaAs/AlGaAs HEMTs are mainly due to two-dimensional electron gas (2DEG) confinement in the channel and also due to the intrinsic characteristics of III-V semiconductors, which are key for modern microwave and power electronics [1], [2]. It is worth noting that HEMTs are also referred to as modulation-doped field effect transistors (MODFETs), as their working principle can be summarized as modulating the concentration of the underlying 2DEG via gate voltage.

Some of the key features of GaN/AlGaN and GaAs/AlGaAs HEMTs are:

- **Electron Confinement**: Electrons in these HEMT structures are confined to a two-dimensional electron gas (2DEG) at the heterointerface. This leads to modified energy levels and superior electronic properties such as high mobility and low noise, which are crucial for RF and microwave applications [3]
- **High Surface-to-Volume Ratio**: The interface properties of GaN/AlGaN and GaAs/AlGaAs play a significant role in device performance. Changes at the surface can impact electron density in the 2DEG, making surface passivation a key area of research to ensure stability and performance for sensing and power devices [4], [5]
- **Mechanical Durability and Thermal Conductivity**: GaN-based HEMTs, in particular, exhibit enhanced robustness and excellent thermal conductivity, making them suitable for high-power and high-temperature environments. This robustness is essential for applications in power amplifiers and radar systems [6]
- **Compatibility with Existing Technologies**: Both GaN and GaAs technologies show potential for integration with mature fabrication processes. GaN HEMTs, for example, are being considered for future advancements in the silicon-dominated power electronics industry due to their superior performance compared to traditional silicon-based transistors [7]

This work comparatively reviews the existing literature on GaN/AlGaN and GaAs/AlGaAs HEMTs. Additionally, based on simulations of these HEMTs, we present results and analyze their performance under various conditions.

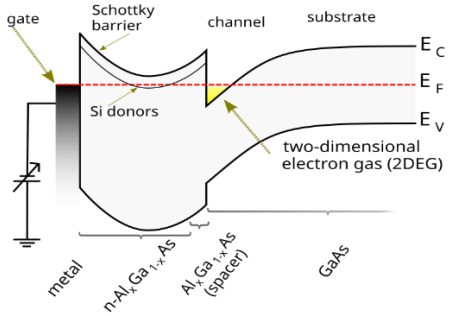

Figure 1. Shows the electron energy band structure of a high electron mobility transistor (HEMT) as a cross-section under the gate electrode. The particular heterostructure depicted in this diagram is the AlGaN/GaN HEMT. Notice the 2DEG channel region depicted in yellow. Adapted from [8].

II. Literature Review: Fabrication, Properties and Applications

A. Process Flow for AlGAs/GaAs and AlGaN/GaN HEMTs

1. Substrate Preparation

- **AlGaAs/GaAs HEMTs**: The process flow begins with semi-insulating GaAs substrates, which are thoroughly cleaned using chemical treatments to remove native oxides. This ensures a defect-free surface for epitaxial growth [8]
- **AlGaN/GaN HEMTs**: Common substrates include sapphire, silicon carbide (SiC), or silicon. An AlN nucleation layer or GaN buffer layer is grown before the active layers to reduce lattice mismatches, enhancing epitaxial quality [9].

2. Epitaxial Growth

- **AlGaAs/GaAs HEMTs**: Molecular beam epitaxy (MBE) or metal-organic chemical vapor deposition (MOCVD) is used to grow high-purity, defect-free layers. The AlGaAs layer, as the barrier, provides a potential well to confine electrons in the GaAs channel, forming a high-mobility 2DEG. The growth is precisely controlled to achieve atomic-level smoothness [10]
- **AlGaN/GaN HEMTs**: MOCVD is the dominant technique due to its scalability. The AlGaN barrier is grown on GaN, and spontaneous polarization effects create a 2DEG without intentional doping. This polarization-induced electron density enhances device performance [11]

3. Device Fabrication

Both HEMT technologies use similar steps for device fabrication, including photolithography for patterning and electron-beam lithography for finer details.

- **AlGaAs/GaAs HEMTs:** Source and drain contacts are made with Ti/Pt/Au, ensuring minimal resistance with the GaAs layer. The gate electrode is often a Schottky contact made of Ni/Au [12]
- **AlGaN/GaN HEMTs:** Due to the robustness of GaN, Ti/Al/Ni/Au stacks are used for ohmic contacts, followed by annealing to achieve excellent conductivity [13]

4. Passivation and Encapsulation

Passivation layers like Si_3N_4 are deposited to prevent surface degradation and reduce gate leakage currents. For GaN devices, passivation is vital in managing surface traps and enhancing reliability under high electric fields [14].

The detailed step-by-step schematic for an AlGaN/GaN HEMT fabrication process flow is illustrated in Figure 2. The process flow for an AlGaAs/GaAs HEMT is similar, albeit simpler. Exact process sequences will differ depending on academic source and fabrication lab/facility. Still, this generic process flow described below for AlGaN/GaN heterostructure gives a technical overview into the general HEMT process sequence that is followed with modifications.

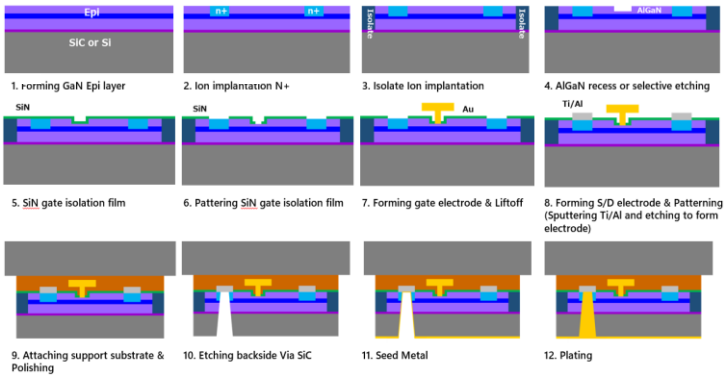

Figure 2. AlGaN/GaN HEMT Manufacturing Process Flow Diagram. A step-by-step process flow schematic for visualizing a typical HEMT fabrication process sequence can be modified as needed. Adapted from [21].

B. Key Properties of AlGaAs/GaAs and AlGaN/GaN HEMTs

<u>Electrical Properties</u>

AlGaAs/GaAs HEMTs:

- The narrow bandgap of GaAs (1.43 eV) results in high electron mobility (~8500 $cm^2/V \cdot s$), contributing to excellent high-frequency performance. However, this comes at the cost of a lower breakdown voltage, limiting their application in high-power scenarios [15].
- Gate leakage currents are minimal due to the Schottky contact, enabling low-noise operation [16].

AlGaN/GaN HEMTs:

- The wide bandgap of GaN (3.4 eV) leads to significantly higher breakdown voltages, making these devices ideal for power applications [17].
- Polarization-induced electron densities in the 2DEG are much higher than in GaAs, enabling higher current densities. However, this comes with challenges like managing higher gate leakage currents and thermal stress [18].

<u>Thermal Properties</u>

AlGaAs/GaAs HEMTs:

Thermal conductivity (~50 $W/m \cdot K$) is sufficient for low-power devices but poses challenges in high-power applications, where heat dissipation becomes critical [19].

AlGaN/GaN HEMTs:

The higher thermal conductivity of GaN (~130 $W/m \cdot K$) supports efficient heat dissipation, making them more reliable under high-power conditions [20].

C. Qualitative Comparison of Materials

The properties of HEMTs discussed so far from the cited literature are tabulated for reference in this section. This provides a summary qualitative comparison between the two HEMT heterostructures (*TABLE 1).*

TABLE 1 Qualitative Comparison of AlGaAs-GaAs and AlGaN_GaN Heterostructures. *Adapted from [15-20]*

Feature	AlGaAs/GaAs HEMTs	AlGaN/GaN HEMTs
Bandgap	Narrow (1.43 eV for GaAs)	Wide (3.4 eV for GaN)
2DEG Density	Moderate	High
Thermal Conductivity	Lower (~50 W/m·K)	Higher (~130 W/m·K)
Breakdown Voltage	Lower	Significantly Higher
High-Frequency Response	Excellent	Excellent at high-power

D. Applications of AlGaAs-GaAs and AlGaN-GaN HEMTs

For completeness, some applications of AlGaAs/GaAs and AlGaN/GaN HEMT heterostructures have been briefly discussed here. These aren't exhaustive, but have been included to motivate the overall study of these devices.

1. AlGaAs/GaAs HEMTs

- Primarily used in low-noise amplifiers (LNAs) for satellite communications and wireless systems due to their high-frequency performance [16]
- Suitable for small-signal amplification in devices where power output is not a critical parameter [17]

2. AlGaN/GaN HEMTs

- Widely employed in high-power RF amplifiers, radar systems, and power conversion circuits. Their ability to handle high voltages and currents enables use in electric vehicles and renewable energy grid [18]
- Emerging use in 5G technology and millimeter-wave applications due to their efficiency at high frequencies and power levels [19]

E. Quantitative Comparison of Materials

A quantitative comparison of GaAs and GaN as semiconducting materials is also imperative to gain insights into the properties and performance of the HEMTs fabricated from these. Such a comparison is done in TABLE 2.

TABLE 2 Quantitative Comparison of Various Compound Semiconducting Materials Corresponding to AlGaAs-GaAs and AlGaN_GaN Heterostructures *(Si values for reference). Adapted [22]*

Parameter	Si	GaAs	GaN	Significance
Band gap (eV)	1.1	1.42	3.39	High operating voltages; High temp. operation
Electron Mobility (cm^2/Vs)	1350	8500	1200	High DC gain; High operating frequency
Dielectric Constant	11.8	13.1	9.0	Lower capacitance; reduces the parasitic delay
Breakdown Electric field (M.V/cm)	0.3	0.4	3.3	Higher operating voltage; High output impedance; Ease of impedance matching
V_{sat} (10^7 cm/s)	1.0	1.0	2.5	High output current density; High DC gain
Thermal conductivity (W/cm.K)	1.5	0.43	1.3	Smaller die size; Efficient heat dissipation

Before concluding this introductory section, an interesting double heterostructure AlGaAs/GaAs structure is discussed here. In course of research, this was encountered by us and the interesting aspect of this structure (*Figure 3)* is that it achieves a 2DEG using ingenious geometry of GaAs and AlGaAs.

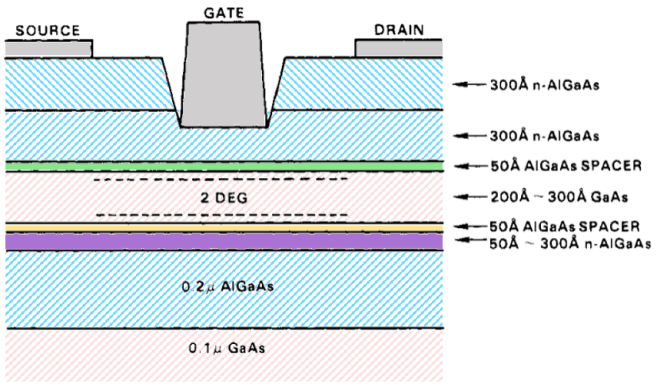

Figure. 3 AlGaAs-GaAs HEMT heterostructure that was deemed notable by the authors. Modified and adapted from [23]

II. Simulations

A. Simulation Platform

For this work, we use the National Taiwan University's (NTU) 1D-DDCC and 2D-DDCC software. DDCC stands for Drift-Diffusion Charge Control solver, and it is essentially a TCAD-based Poisson-Schrodinger solver. The two levels of complexity are the one-dimensional and the two-dimensional DDCCs. While the two platforms differ in complexity, there are a certain number of parameters that can be varied for each.

Key DDCC Input Parameter Sections

1. Material Properties – *Epi layers, polarization, doping carrier concentration, x-y composition ($A_xB_{(1-x)}C_yD_{(1-y)}E$)*
2. Material Database – *Consists of the pre-loaded database for thermal coefficients, bandgaps & mobilities (Figure 4)*
3. Range Builder – *Layered ranges, empty ranges, contact region setting tool, GUI etching tool (Figure 4)*
4. Meshing – *Important for accuracy vs. speed trade-off for the Poisson-Schrodinger equation solver at each grid point*

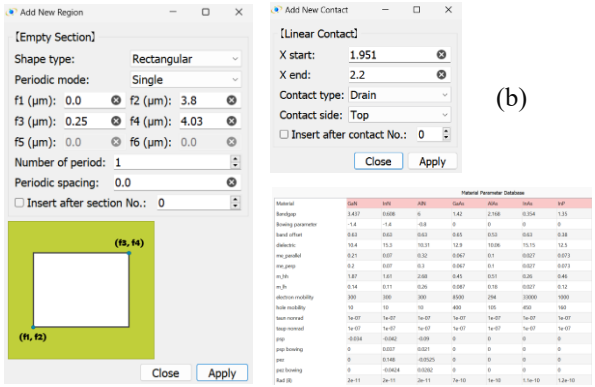

(a) (b) (c)

Figure 4. Shows the view of the NTUs 2D-DDCC platform's input parameter windows (a) Shows the etching empty layer adding tool window (b)Shows the contact setting window (c) Shows the comprehensive material database pre-loaded in the platform for a wide range of materials, primarily III-V ones

In the following sections, the various sets of simulations carried out by us are discussed. 1D-DDCC is used for HEMT heterostructure simulation to get comparative 2D plots, while 2D-DDCC is used to compute more complicated 2D HEMT simulations.

B. 1D-DDCC Heterostructure Simulations:

Before moving on to more complicated simulations and attempting detailed analysis, the first step is to compare and analyze simpler AlGaAs/GaAs and AlGaN/GaN heterostructures. This was done in 1D-DDCC, and the comparative results are discussed in this section.

The comparison of HEMTs for the two cases is shown in *Figure 5* below. Note that for succinct analysis, we have simulated the interfaces here.

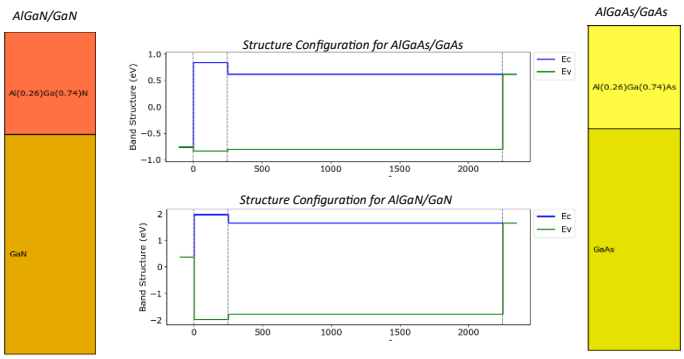

Figure 5. The material composition schematics for the two heterostructures of AlGaAs-GaAs and AlGaN-GaN HEMTs are at the two ends of this figure. The structure-configuration diagram for each case depicts the bandgap of both heterostructures. Individual components have been labelled. These are adapted from the GUI of the 1D-DDCC input parameter setting window.

Note from *Figure 5* that the chosen composition for the interfaces of both the heterostructures is analogous, but the bandgap values for AlGaN/GaN are visibly higher than those of AlGaAs/GaAs, which conforms to theory.

Figure 6 plots the band diagram at zero bias for each case. In the case of AlGaN/GaN, note the highlighted triangular 2DEG evident at the interface. Thus, this simulation also confirms the theoretical presence of a 2DEG at the AlGaN-GaN interface due to polarization effects. This is absent in AlGaAs-GaAs at zero bias, but in the third diagram, at a gate bias of +1 V, we can see a 2DEG forming at the interface.

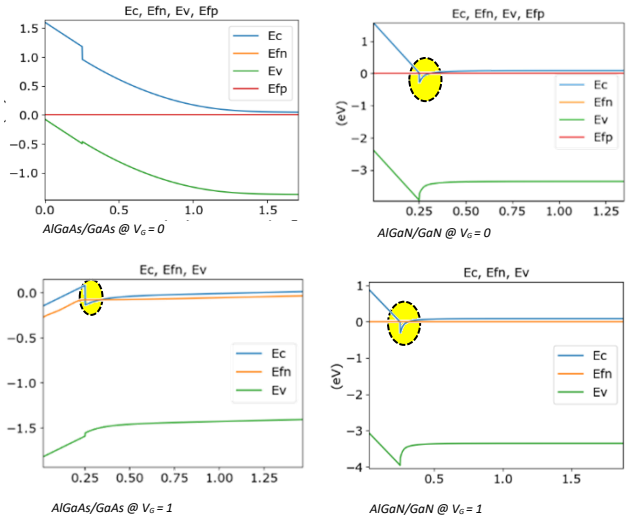

Figure 6. The band diagrams of AlGaAs-GaAs and AlGaN-GaN HEMT interfaces are simulated at two different values of V_G – zero bias and +1 V

For the AlGaN-GaN HEMT interface, it is evident that the 2DEG exists irrespective of the bias, and the only noticeable change is that all energy levels move down due to the applied bias. For the AlGaAs-GaAs interface, the contrast is more marked. The 2DEG that did not exist at zero bias becomes evident at +1 V bias.

The presence of 2DEG indicates that the interface has a conducting channel. From simulations, it is evident that the 2DEG for the AlGaN-GaN interface only disappears at a highly negative applied bias. Hence, this indicates the *normally-ON* tendency discussed widely in the context of GaN HEMTs.

Now, for the applied bias V_G, we plot the left current against it. This would give a semblance of actual HEMT behaviour due to the limitations on contact functionalization in 1D-DDCC. Note that further ahead, when the AlGaN-GaN HEMT is simulated with 2D-DDCC, we get much more accurate data. The log(I) vs. VG characteristics have been plotted for both interfaces in *Figure 7.* The gate control in the case of AlGaN-GaN HEMT is tighter because, over a range of 1 V, the variation in log(I) is from 10^{-4} to 10^{4} A.cm^{-2} (can be normalized to the area without loss of generality). On the other hand, for a similar change in the current for the AlGaAs-GaAs HEMT, a variation of around 2 volts is observed.

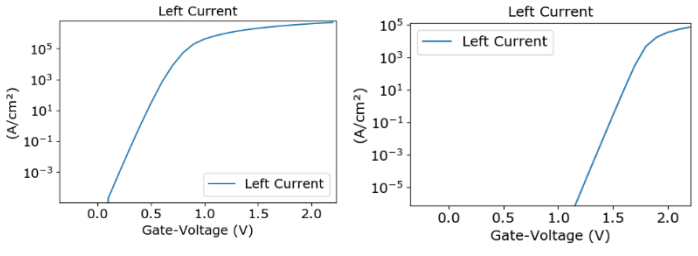

(a) (b)

Figure. 7 (a) logI-V_G characteristics, for AlGaAs-GaAs heterostructure (b) logI-V_G curve, for AlGaN-GaN heterostructure. Note gate control in the two cases – voltage change per decade current

C. 2D-DDCC simulations

After completing most of the basic 2D analysis of the heterostructures, we planned to do an extensive 2D modeling of HEMTs on 2D-DDCC. This was done for the AlGaN-GaN heterostructure primarily because of its complexity, novelty, and more readily available resources for this platform. The structure on which the model was based is described in [24], and a schematic is shown in *Figure 8.*

This structure was adapted into the input windows of 2D-DDCC as introduced earlier, and the contact, empty regions and layered regions were subsequently added, with appropriate dimensions. The input GUI structure is shown in *Figure 9.* The relative dimensions of the channel layers is much smaller than the body, and thus, for clarity, a blown-up view of the top layer is shown as well in *Figure 9.*

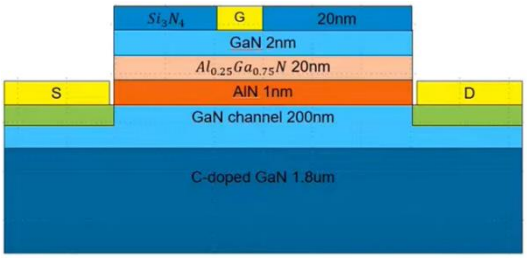

Figure 8. The schematic of the AlGaN-GaN HEMT simulated on 2D-DDCC

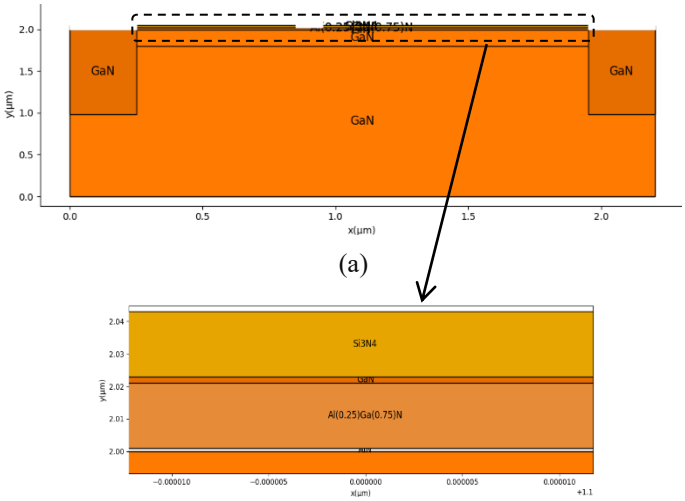

(a)

(b)

Figure 9. The input GUI window showing the device structure which is being simulated, after setting doping, etching relevant layer, and setting contacts.

Based on the above structure, simulation parameters were set in the multiple input spaces. These included updating polarization values, setting trap charges and also uploading field-dependent mobility, which was available with the documentation of the 2D-DDCC software package.

Following this, a meshing strategy was set-up. Two sets of simulations were run, one with coarse meshing and one with fine meshing. The general view of the mesh is depicted in *Figure 10.* The coarse meshing strategy had a run time of several minutes, but the plot obtained (*Figure 11a.)* was discrete. The finer meshing strategy had a runtime of several hours, but a smoother plot (*Figure 11b)* was obtained.

The finer meshing strategy also allowed for exploration of 3D field plots and also a consolidated plot of E_C variation at multiple values of V_G. These are captured in *Figures 12 &13.*

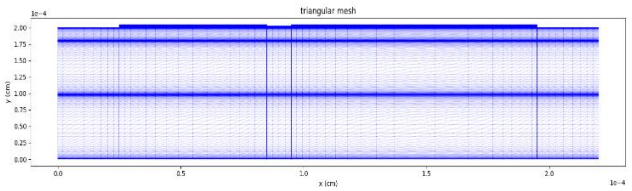

Figure 10. The triangular mesh grid in the solver is based on the structure shown in the previous figure. A fine and coarse meshing strategy were both employed.

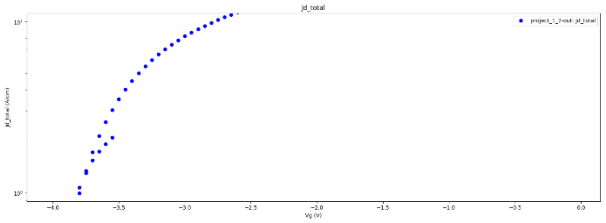

(a)

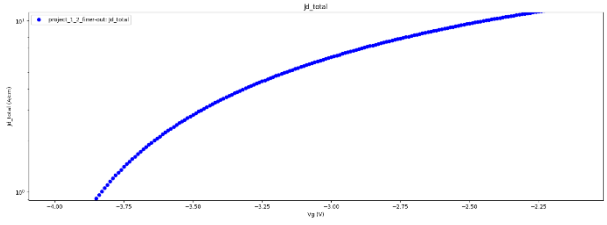

(b)

Figure 11. log(I_D) vs. V_G transfer characteristics for AlGaN-GaN HEMT heterostructure simulated in 2D-DDCC with: (a) coarse meshing, and (b) fine meshing. The accuracy vs. time trade-off is stark – (a) took less than an hour of CPU time, while (b) took several hours of CPU time

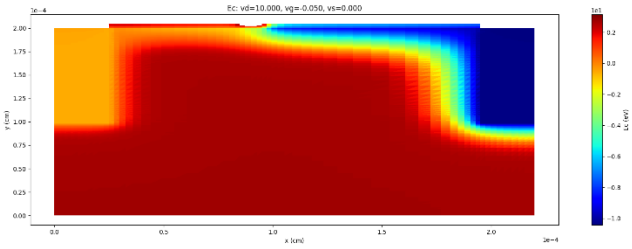

(a)

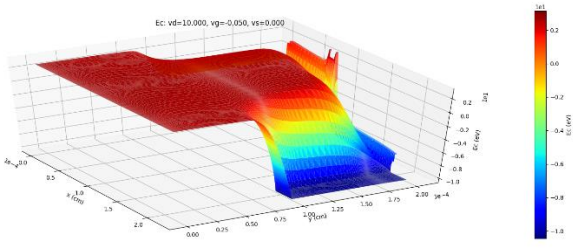

(b)

Figure 12. Heat map of E_C values across device structure in (a) 2D & (b) 3D

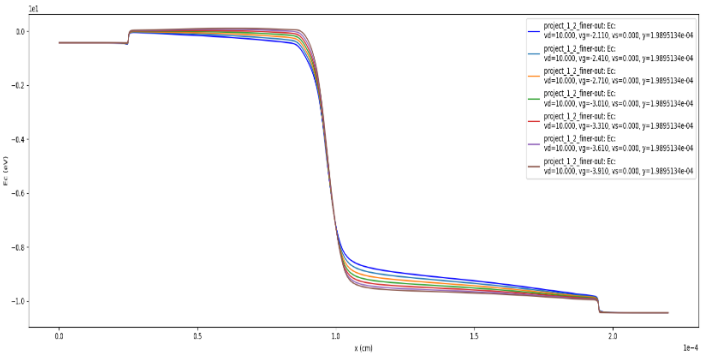

Figure 13. Variation of the conduction band of the HEMT at fixed V_D and varying values of V_G. E_C flattens with applied negative gate voltage to offset the effect of 2DEG – flatband

CONCLUSION

HEMT technology has become a forerunner in modern electronic device industry. III-V compounds take primacy in key industry like HEMTs and LEDs. The major materials used for HEMTs include GaAs and GaN, with GaAs being the traditionally explored material. Through this work, we can critically analyze the differences between the two and comment on the supremacy of nitride performance across multiple parameters. The DDCC simulation study conducted is of great pedagogical and analytical value and promises great scope of being expanded upon in the future for more directed applications and diverse material sets.

REFERENCES

[1] Y. Zhang, A. K. Wong, "Advances in III-V Semiconductor Heterostructures for High-Power Electronics," Journal of Applied Semiconductor Physics, vol. 56, no. 3, pp. 100-115, 2021.

[2] M. T. Nakamura, "Overview of GaN-Based Power Electronics," International Journal of Power Electronics, vol. 45, no. 6, pp. 237-245, 2020.

[3] H. Liu, C. Kim, "2DEG Transport Properties in AlGaN/GaN and AlGaAs/GaAs HEMTs," IEEE Transactions on Electron Devices, vol. 68, no. 5, pp. 1556-1562, 2019.

[4] P. Sharma, L. Hsu, "Surface Passivation Techniques for High-Performance HEMTs," Materials Science and Engineering B, vol. 223, pp. 134-142, 2018

[5] S. R. Lee, J. Patel, "Interface Engineering in GaN/AlGaN HEMTs," Semiconductor Interface Journal, vol. 12, no. 4, pp. 78-86, 2021.

[6] T. Kowalski, "Thermal Management in GaN-Based HEMTs," Progress in Power Semiconductor Devices, vol. 34, no. 8, pp. 45-60, 2020.

[7] D. K. Gupta, "Integration of GaN HEMTs with Silicon Platforms: Opportunities and Challenges," Electronics & Materials Research, vol. 18, no. 2, pp. 99-108, 2019.

[8] D. J. Widiger, I.C. Kizilyalli, K. Hess, J.J. Coleman, "Two-dimensional transient simulation of an idealized high electron mobility transistor," Electron Devices, IEEE Transactions on. Vol. 32 Issue 6, 1985, pp. 1092-1102

[9] Doerk, G. S., Carraro, C., & Maboudian, R. (2010). Single nanowire photovoltaics with silicon-based single- and double-sided junctions. ACS nano, 4(8), 4908-4914.

[10] Lu W, Lieber CM. Nanoelectronics from the bottom up. Nat Mater. 2007 Nov;6(11):841-50. doi: 10.1038/nmat2028. PMID: 17972939.

[11] Tian B, Cohen-Karni T, Qing Q, Duan X, Xie P, Lieber CM. Threedimensional, flexible nanoscale field-effect transistors as localized

bioprobes. Science. 2010 Aug 13;329(5993):830-4. doi: 10.1126/science.1192033. PMID: 20705858; PMCID: PMC3149824.
[12] Zheng G, Patolsky F, Cui Y, Wang WU, Lieber CM. Multiplexed electrical detection of cancer markers with nanowire sensor arrays. Nat Biotechnol. 2005 Oct;23(10):1294-301.
[13] D. J. Widiger, I.C. Kizilyalli, K. Hess, J.J. Coleman: Two-dimensional transient simulation of an idealized high electron mobility transistor. in: Electron Devices, IEEE Transactions on. Vol. 32 Issue 6, 1985, pp. 1092-1102
[14] Anderson, R. T., & Miller, J. P. (2011). High-frequency performance of GaAs-based HEMTs: A review of challenges and applications. Journal of Semiconductor Research, 24(3), 135-145
[15] Adesida and H. Morkoç, "Lattice mismatch management in AlGaN/GaN systems for high-performance HEMTs," IEEE Transactions on Electron Devices, vol. 48, no. 3, pp. 500-506, 2001.
[16] Yoshida, K., & Tanaka, M. (2014). The potential of wide bandgap materials in high-power electronics: A focus on AlGaN/GaN HEMTs. Applied Physics Reviews, 21(2), 98-105.
[17] Chen, L., & Zhao, W. (2013). Schottky contact mechanisms and their impact on noise performance in AlGaAs/GaAs HEMTs. IEEE Transactions on Electron Devices, 60(7), 2486-2493.
[18] Kumar, P., & Lin, D. J. (2015). Challenges in managing polarization-induced electron densities in AlGaN/GaN HEMTs. Journal of Electronic Materials, 44(8), 2902-2910.
[19] Park, S., & Lee, C. H. (2016). High thermal conductivity in GaN and its role in high-power device reliability. Journal of Applied Physics, 119(3), 033502..
[20] Mohd Faizol *et al*. “Chip-level thermal management in GaN HEMT: Critical review on recent patents and inventions,” *Microelectronic Engineering*,doi.org/10.1016/j.mee.2023.111958
[21] “GaN HEMT Fabrication Flow,” Vacuum Magazine. ULVAC. Japan. https://www.ulvac.co.jp/wiki/en/process_g_gan_hemt/
[22] Nandha Kumar Subramani. “Physics-based TCAD device simulations and measurements of GaN HEMT technology for RF power amplifier applications.” Electronics. Université de Limoges, 2017. English. f
[23] N. H. Sheng, C. P. Lee, R. T. Chen and D. L. Miller, "GaAs/AlGaAs double heterostructure high electron mobility transistors," *1984 International Electron Devices Meeting*, USA, 1984, pp. 352-355
[24] Yuhren Wu (2022). “GaN HEMT ITRI Demo.”